VALIDATION OF NON-AXISYMMETRIC TERMS IN 3-D VISCOUS FLOW ANALYSIS FOR HIGH SPEED AXIAL COMPRESSORS

Kaldellis J.K.[1], Georgantopoulos G.A.

Hellenic Air Force Academy, Dept. of Aerodynamics

Abstract

The viscous 3-D flow method developed by the authors during the last years has been proven to be an appropriate and efficient way of treating complex flow fields in single and multi-stage machines. According to this model the complete form of the time averaged Navier-Stokes equations is pitch-wise integrated. Subsequently, the real value of a quantity is expressed as the sum of the circumferentially mean value of the quantity and a fluctuation term, describing the distribution of the quantity in the peripheral direction. In the present work, a complete theoretical analysis concerning the passage-averaged model in an orthogonal curvilinear axisymmetric coordinate system is described. The non-uniformity terms are first evaluated using various available experimental data. Then the most important terms are modelled, in order to be included in the complete viscous flow method, keeping the same order of the computational requirements. Finally, the impact of the assessed non-axisymmetric terms on the quality of the calculation results is demonstrated, by comparing the prediction results with and without the contribution of the "apparent stresses", using several high speed axial compressor configurations.

Nomenclature

b	peripheral blockage factor
B	(=b.R)
$\vec{D}$	deficit force vector
DM,DU	meridional and peripheral component of the total blade deficit force
DM_1,DU_1	spanwise integrated meridional and peripheral deficit force components
$\vec{F}$	force vector
k_m,k_n	curvature of m-,n- lines
$\vec{L}$	blade pressure force
p	static pressure
R	radius
$\vec{S}$	blade shear (dissipative) force
s	entropy
T	temperature
$\vec{V}$	absolute velocity vector
$\vec{W}$	relative velocity vector
z*	number of blades
β	angle between meridional -m and primary flow direction
β'	blade angle
δ'	normal blade angle
ε_D	deficit force deviation angle
Θ	peripheral position of the blade surfaces
(θ,m,n)	coordinates of an orthogonal curvilinear axisymmetric system
$\vec{\xi}$	vorticity vector
ϱ	density
τ_{ij}	components of shear stresses
ϕ	angle between the meridional direction and the axis of the machine
$\vec{\omega}$	angular velocity vector

Subscripts

e	external flow
p,s	pressure and suction side of the blade
(u,m,n)	components in a curvilinear axisymmetric orthogonal coordinate system

Superscripts

(-)	peripheral mean value
'	peripheral fluctuation values

1. Introduction

The viscous 3-D flow method developed by the authors during the last years [1], [2] has been proven to be an appropriate and efficient way of treating complex flow fields in single and multi-stage machines, being also an alternative answer to the use of the time consuming full Navier

(1) also Technological Education Institute of Piraeus; Permanent address: Pontou 58, 16777 Greece.

Stokes approach. In the proposed model special emphasis was put on the distinction between the existing axisymmetric flow models and the proposed circumferentially averaged one, developed from first principles. More precisely, in our early work [1] the basic principles of the Circumferentially Averaged Model (CAM) were established. According to this model the complete form of the time averaged Navier-Stokes equations is pitch-wise integrated. Subsequently, the real value of a quantity is expressed as the sum of the circumferentially mean value of the quantity and a fluctuation term, describing the distribution of the quantity in the peripheral direction.

The application of the CAM on the Navier-Stokes equations leads to the appearance of some additional terms like the values of the flow parameters on the blade suction and pressure side (blade force) and the so called "apparent" stresses. The apparent stresses usually include the circumferentially averaged fluctuation terms and are called so in an analogy to the Reynolds stresses, describing the turbulence fluctuation terms [3],[4]. The so called "apparent stresses" are commonly assumed responsible for the limited performance of various early calculation methods and for the existing discrepancies between the calculated and the experimental data. Only by neglecting the blade force terms and the corresponding apparent stresses the equations of the CAM coincide with the equations valid for the axisymmetric model. Besides, during the development of the governing equations, we have **not** accepted that the axisymmetric surfaces used in the curvilinear coordinate system coincide with the flow surfaces. Therefore, the normal velocity components are included in our analysis for both the external and the real flow field.

In the present work, a complete theoretical analysis concerning the passage-averaged model in an orthogonal curvilinear axisymmetric coordinate system is described. The non-uniformity terms are first evaluated using various available experimental data. Then the most important terms are modelled, in order to be included in the complete viscous flow method, keeping the same order of the computational requirements. Finally, the impact of the assessed non-axisymmetric terms on the quality of the calculation results is demonstrated, by comparing the prediction results with and without the contribution of the "apparent stresses".

2. Theoretical Model-Deficit Force Terms

During the development of our method special attention was paid in order to use the complete form of the corresponding equations. Therefore, after applying the CAM on the governing flow equations we get the equations presented in Appendix One. Some of the most important non-axisymmetric terms appearing in the CAM are the terms describing the blade force exerted between the fluid and the bladings. More precisely, the three components of the real force between the blade and the fluid are defined as:

$$F_i = L_i + S_i \qquad (i=u,m,n) \tag{1}$$

with

$$L_u = \frac{z^*}{2\pi}\cdot(p_p - p_s) \tag{2}$$

$$L_i = \frac{R\cdot z^*}{2\pi}\cdot\left(p_s\cdot\frac{\partial\theta_s}{\partial i} - p_p\cdot\frac{\partial\theta_p}{\partial i}\right) \quad (i=m,n) \tag{3}$$

and

$$S_i = \frac{z^*}{2\pi}\cdot(\tau_{ui_s} - \tau_{ui_p}) - R\cdot\frac{z^*}{2\pi}\cdot\left[\left(\tau_{mi_s}\cdot\frac{\partial\theta_s}{\partial m} - \tau_{mi_p}\cdot\frac{\partial\theta_p}{\partial m}\right) + \left(\tau_{ni_s}\cdot\frac{\partial\theta_s}{\partial n} - \tau_{ni_p}\cdot\frac{\partial\theta_p}{\partial n}\right)\right] \quad (i=u,m,n) \tag{4}$$

Assuming relatively thin blades, which is quite realistic for compressor cascades especially for high speed machines, and defining the static pressure difference "Δp" between the pressure and the suction side of the blade as:

$$\Delta p = p_p - p_s \tag{5}$$

equations (2) and (3) are written as:

$$L_u = \frac{z^*}{2\pi}\cdot\Delta p \tag{6}$$

$$L_m = \frac{-R\cdot z^*}{2\pi}\cdot\Delta p\cdot\frac{\partial\bar{\theta}}{\partial m} \tag{7}$$

$$L_n = \frac{-R\cdot z^*}{2\pi}\cdot\Delta p\cdot\frac{\partial\bar{\theta}}{\partial n} \tag{8}$$

Using the blade geometry we can estimate the above mentioned derivatives of the blade mean camber as:

$$\frac{\partial\bar{\theta}}{\partial m} = \frac{\tan\beta'}{R} \tag{9}$$

$$\frac{\partial\bar{\theta}}{\partial n} = -\frac{\tan\beta'\cdot\tan\delta'}{R} \tag{10}$$

where "β'" and "δ'" are the blade angles, see also [5], [6]. Combining equations (6),(7) and (8) we can relate the three blade pressure force components as:

$$L_m = -L_u \tan\beta' \tag{11}$$

$$L_n = L_u \tan\beta' \tan\delta' \tag{12}$$

According to equations (11) and (12) we may conclude that the blade pressure force is normal to the blade surface. Additionally, we can calculate [2] the three blade pressure force components as soon as the static pressure difference is known along with the blade geometry. Using now the same relations for the external "inviscid" flow field we can derive the corresponding relations concerning the blade pressure deficit force, as it appears in our model, i.e.:

$$\Delta L_m = -\Delta L_u \tan\beta' \tag{13}$$

$$\Delta L_n = \Delta L_u \tan\beta' \tan\delta' \tag{14}$$

$$\Delta L_u = \frac{z^*}{2\pi}\cdot(\Delta p_e - \Delta p) \tag{15}$$

where "Δp_e" is the corresponding external flow pressure difference between the blade surfaces. In order to estimate the three deficit force components we have to calculate the change of the blade loading due to the interaction between the secondary flow field and the blade shear layers [2].

In the following figure [1] the spanwise distributions of the peripheral component of the external and the real flow blade pressure force are presented for the midchord of a highly loaded compressor cascade, Flot case B', already analyzed by the authors [7]. As we can easily see from these figures the real pressure force is less than the external one only near the endwall, while it is greater than at the major part of the channel. Additionally, for this cascade test case the external pressure force is constant all over the span. Note that the difference between the real and the external force is quite important, especially near the midchord of the blade, a fact that is also verified by the measurements presented [8] by Flot (1975). Despite the scattering of the experimental points, the predicted force by the blade-to-blade shear flow model [2] describes accurately enough the experimental trends. Similar pressure force profiles are given [9] by Storer and Cumpsty (1990) for rotor cases without tip clearance effects.

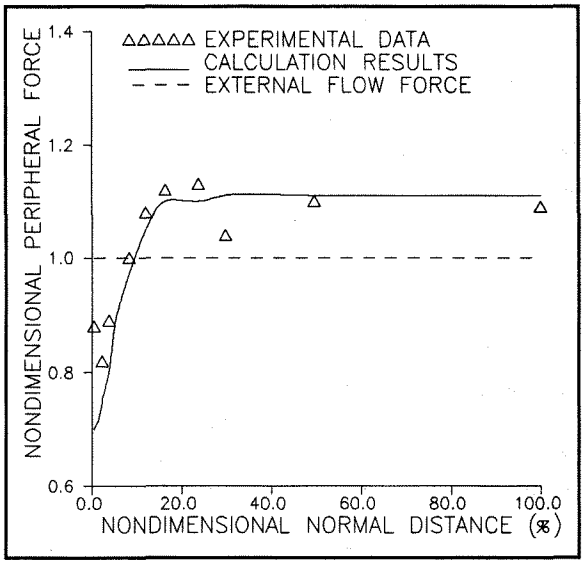

Figure 1: Spanwise distribution of the peripheral component of the blade pressure force, "Lu", "Lu_e".

Passing now to the shear (dissipative) part of the blade force "$\bar{S}$", it is necessary to calculate the complete shear stress tensor "τ_{ij}" at the suction and the pressure side of the blade, eq.(4). In order to avoid this really painful task we may use equivalently the entropy-shear force relation given by [10] Hawthorne (1964), which however assumes implicitly that the rothalpy of the flow field is constant along a streamline. More precisely, for the deficit shear force components one may write:

$$\Delta S_i = \frac{\bar{T}}{1+\tan^2\beta+\tan^2\phi}\cdot\frac{\partial s}{\partial i} \quad (i=m,n) \tag{16}$$

$$\Delta S_u = \frac{\bar{T}}{1+\tan^2\beta+\tan^2\phi}\cdot\frac{\partial s}{R\cdot\partial\theta} \tag{17}$$

Subsequently,using the analysis [11] by Kaldellis and Ktenidis (1990) the complete peripheral component of the deficit force "D_u" is given by the momentum equation in the peripheral direction as a function of the secondary vorticity components, i.e:

$$D_u = R\cdot(\bar{\rho}\cdot\bar{W}_m\cdot\bar{\xi}_n^* - \bar{\rho}_e\cdot\bar{W}_{m_e}\cdot\bar{\xi}_{n_e}^*) - R\cdot(\bar{\rho}\cdot\bar{W}_n\cdot\bar{\xi}_m^* - \bar{\rho}_e\cdot\bar{W}_{n_e}\cdot\bar{\xi}_{m_e}^*)$$

$$+2\omega\cdot B\cdot[\sin\phi\cdot(\bar{\rho}_e\cdot\bar{W}_{m_e} - \bar{\rho}\cdot\bar{W}_m) + \cos\phi\cdot(\bar{\rho}_e\cdot\bar{W}_{n_e} - \bar{\rho}\cdot\bar{W}_n)]$$

$$-B\cdot[\frac{\partial lnb}{\partial m}\cdot(\bar{\rho}_e\cdot\bar{W}_{m_e}\cdot\bar{W}_{u_e} - \bar{\rho}\cdot\bar{W}_m\cdot\bar{W}_u) + \frac{\partial lnb}{\partial n}\cdot(\bar{\rho}_e\cdot\bar{W}_{n_e}\cdot\bar{W}_{u_e} -$$

$$-\bar{\rho}\cdot\bar{W}_n\cdot\bar{W}_u)] + \frac{\partial(B\cdot\bar{\tau}_{uu})}{\partial m} + b\cdot(\cos\phi\cdot\bar{\tau}_{nu} + \sin\phi\cdot\bar{\tau}_{mu}) \tag{18}$$

Consequently, the "ΔS_u" term can also be predicted as the difference between the complete peripheral deficit force "D_u" and the blade pressure force component "ΔL_u",using the secondary vorticity components and the change of the blade loading due to the secondary flow field, i.e.:

$$\Delta S_u = D_u - \Delta L_u \qquad (19)$$

The "ΔS_u" term expresses the impact of the secondary losses on the blade loading in the peripheral direction, and may modify significantly the energy exchange (**added work term**) according to the analysis by [5] Kaldellis (1994) via the energy conservation equation.

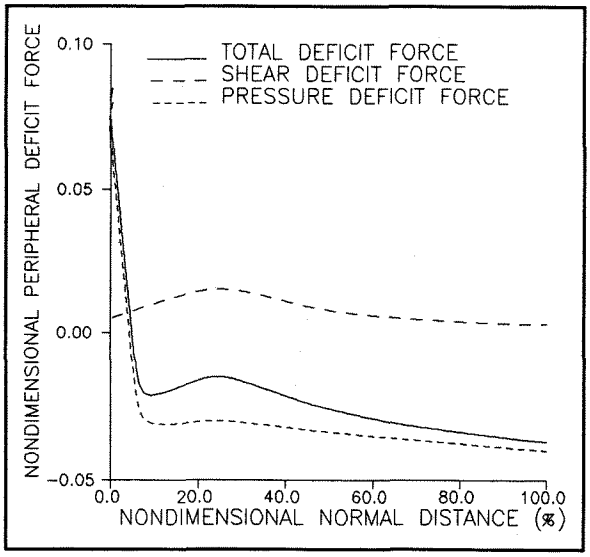

Figure 2: Spanwise distribution of the peripheral components of deficit force.

In the figure [2] the predicted peripheral components of the pressure, the shear and the total deficit force spanwise distributions are presented near the exit of the above mentioned compressor cascade, non-dimensionalized by the external force value. As it is expected the dissipative deficit force component is positive and its distribution is in accordance with the 3-D loss distribution given [2] for the same station of the cascade. On the other hand the pressure deficit force is negative excluding the wall region and takes much more greater values than the corresponding shear deficit force. Therefore, the complete deficit force is dominated by the pressure deficit force component. It is interesting also to mention that the peripheral component of the shear force is computed using equation (19) and not equation (17). At the same time the other two deficit shear force components (ΔS_m, ΔS_n), can be predicted using the loss distribution in the meridional and the normal flow directions.

Several (deficit) force models are presented during the last thirty years depending the desired accuracy and the available experimental and computational results. L.H. Smith (1955) seems to be the first who underline the importance of the deficit force terms without however to propose a complete simulation model. Accordingly, the formulations used assume either that the force vector is normal to the blade surface or that the deficit force components are very small. Mellor and Wood (1971) relate the complete deficit force vector (for all the blade) with the components of the external velocity via an empirical coefficient "ε", i.e.

$$\bar{W}_{m_{ref}} \cdot DM + (1-\epsilon) \cdot \bar{W}_{u_{ref}} \cdot DU = 0 \qquad (20)$$

while the normal (radial) deficit force component was neglected. Horlock and Perkins (1974) propose a relatively accurate expression of the spanwise integral of the peripheral deficit force, from a simplified form of the integral momentum equation in the peripheral direction, i.e.:

$$DU_1 = B_w \cdot \rho_{e_w} \cdot W_{e_{ref}}{}^2 \cdot (\delta^*_s + \theta_{ss}) \cdot \frac{\partial \bar{\beta}_{e_w}}{\partial m} \qquad (21)$$

In this way for first time the peripheral deficit force component was quantitatively related with the secondary flow field.

Comte et al., 1981, starting from the expression given by Mellor and Wood (1971) for the spanwise integrated deficit force components, they assumed that the deficit force is normal to the mean blade camber angle, i.e.:

$$DM_1 + \tan\beta' \cdot DU_1 = 0 \qquad (22)$$

neglecting also the radial deficit force component. The same expression was also used by Leboeuf and Brochet (1985) for the analysis of a transonic axial compressor with reasonably good results. However, this expression was modified by Brochet and Falchetti (1987) using an empirical coefficient "ε" (found by numerical tests) in order to convergent their secondary flow code in multistage axial compressor flow cases. However, the arbitrary chosen coefficient "ε" limits the applicability of that method.

Recapitulating, we can say that the change of the force exerted between the blades and the fluid can be split in a pressure and a shear (dissipative) term. For the pressure deficit force component the equations (13) (14) and (15) are almost strictly mathematically valid, and express the change of the blade loading, mainly due to the interaction between the secondary flow field and the blade shear layers. For the shear deficit force component one has to take into account the loss distribution through out the machine. Taking into account that the peripheral momentum equation and the meridional vorticity transport one are not independent we can estimate the complete deficit force component from equation (18) and subsequently the corresponding dissipative force component from equation (19). On the other hand the meridional deficit force component is related with the peripheral one, using the following equation:

$$D_m = -D_u \tan(\beta' - \epsilon_D) \qquad (23)$$

taking also into account [1] the deviation from the normal to the blade condition. As we can see from equations (16),(17) and (23) the coefficient "ε_D" expresses the relation between the primary flow and the secondary flow losses. Thus every predescribed relation (empirical or numerical) between the meridional and the peripheral deficit force components is an implicit constraint between the primary flow and the secondary flow losses. Therefore, by taken [12] the parameter "ε" equal to 0.7 in order to achieve convergence, one impose a strong relation between the secondary loss and the primary flow loss (secondary loss and profile loss), a fact that may lead to incorrect loss level due to the predescribed loss relation. Typical predicted spanwise mean "ε_D" values are given in the next figure [3], concerning the deficit force distribution through the above mentioned highly loaded compressor cascade.

For this cascade test case the blade angle "β'" is constant, therefore the spanwise mean deficit force deviation angle "ε_D" can be easily predicted using equation (23) and the corresponding values of the spanwise mean peripheral and meridional deficit force components. As we can see from figure [3] the deficit force deviation angle is negative over the first 60% of the blade and is increased monotonically from the leading edge to the trailing edge, taking values between -6° to +3°. The same behaviour is also shown by the experimental points. Similar (but smaller than) values are given also [13] for the deficit force deviation angle concerning the blade force in a cascade case at the presence of tip clearance. Finally, keep in mind that the blade mean deficit force deviation angle is approximately zero, a fact that validates the assumption used by Mellor and Wood (1971) in their early work [14].

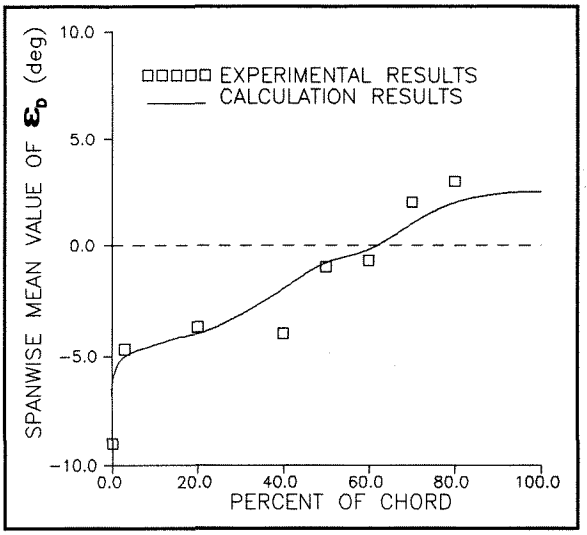

Figure 3: Distribution of the spanwise mean value of the deficit force deviation angle.

Finally, for the normal force component, one have to use equations (14) and (16). However, during our calculations the "ΔS_n" is found to be very small (at least for axial compressor cases) while the "ΔL_n" term can be taken to be zero in the absence of dihedral effects ($\delta' \approx 0$.).

3. Theoretical Model-Fluctuation Terms

The second group of non-axisymmetric terms appearing in the circumferentially averaged equations, given in Appendix One, after the application of the CAM are the apparent stress terms which describe the deviation of the flow from the axisymmetry. What is more impressive is that although the deficit force terms almost vanish near the exit of bladed regions and in the corresponding free spaces, the apparent stresses are present even in free spaces, since the flow field presents a non-axisymmetric character due to the three-dimensional airfoil wakes and the existing three-dimensional endwall shear layers. In the following the corresponding fluctuation terms "Δ_o, Δ_u, Δ_m, Δ_n" are presented as they appear in the governing flow equations.

Mass Conservation Equation

$$\Delta_o=\frac{1}{b}\cdot\left[\frac{\partial}{\partial m}(b\cdot R\cdot\overline{\rho'\cdot W'_m})+\frac{\partial}{\partial n}(b\cdot R\cdot\overline{\rho'\cdot W'_n})\right] + R\cdot(k_n\cdot\overline{\rho'\cdot W'_m}+k_m\cdot\overline{\rho'\cdot W'_n}) \quad (24)$$

Momentum Equation-Peripheral Direction

$$\Delta_u=-\frac{1}{b}\cdot\frac{\partial[B\cdot(\bar{\rho}\cdot\overline{W'_m\cdot W'_u}+\bar{W}_m\cdot\overline{\rho'\cdot W'_u}+\bar{W}_u\cdot\overline{\rho'\cdot W'_m}+\overline{\rho'\cdot W'_m\cdot W'_u})]}{\partial m}$$
$$-\frac{1}{b}\cdot\frac{\partial[B\cdot(\bar{\rho}\cdot\overline{W'_n\cdot W'_u}+\bar{W}_n\cdot\overline{\rho'\cdot W'_u}+\bar{W}_u\cdot\overline{\rho'\cdot W'_n}+\overline{\rho'\cdot W'_n\cdot W'_u})]}{\partial n}$$
$$-\cos\phi[\bar{\rho}\cdot\overline{W'_u\cdot W'_n}+\bar{W}_u\cdot\overline{\rho'\cdot W'_n}+\bar{W}_n\cdot\overline{\rho'\cdot W'_u}+\overline{\rho'\cdot W'_u\cdot W'_n}+2\omega\cdot R\cdot\overline{\rho'\cdot W'_n}]$$
$$-\sin\phi[\bar{\rho}\cdot\overline{W'_u\cdot W'_m}+\bar{W}_u\cdot\overline{\rho'\cdot W'_m}+\bar{W}_m\cdot\overline{\rho'\cdot W'_u}+\overline{\rho'\cdot W'_u\cdot W'_m}+2\omega\cdot R\cdot\overline{\rho'\cdot W'_m}]$$
$$-R\cdot[k_n\cdot(\bar{\rho}\cdot\overline{W'_u\cdot W'_m}+\bar{W}_u\cdot\overline{\rho'\cdot W'_m}+\bar{W}_m\cdot\overline{\rho'\cdot W'_u}+\overline{\rho'\cdot W'_u\cdot W'_m})$$
$$+k_m\cdot(\bar{\rho}\cdot\overline{W'_u\cdot W'_n}+\bar{W}_u\cdot\overline{\rho'\cdot W'_n}+\bar{W}_n\cdot\overline{\rho'\cdot W'_u}+\overline{\rho'\cdot W'_u\cdot W'_n})] \quad (25)$$

Momentum Equation-Meridional Direction

$$\Delta_m=-\frac{1}{b}\cdot\frac{\partial[B\cdot(\bar{\rho}\cdot\overline{W'^2_m}+2\bar{W}_m\cdot\overline{\rho'\cdot W'_m}+\overline{\rho'\cdot W'^2_m})]}{\partial m}$$
$$-\frac{1}{b}\cdot\frac{\partial[B\cdot(\bar{\rho}\cdot\overline{W'_m\cdot W'_n}+\bar{W}_m\cdot\overline{\rho'\cdot W'_n}+\bar{W}_n\cdot\overline{\rho'\cdot W'_m}+\overline{\rho'\cdot W'_m\cdot W'_n})]}{\partial n}$$
$$+\sin\phi(\bar{\rho}\cdot\overline{W'^2_u}+2\bar{W}_u\cdot\overline{\rho'\cdot W'_u}+\overline{\rho'\cdot W'^2_u}+2\omega\cdot R\cdot\overline{\rho'\cdot W'_u})$$
$$-R\cdot[2k_m\cdot(\bar{\rho}\cdot\overline{W'_n\cdot W'_m}+\bar{W}_n\cdot\overline{\rho'\cdot W'_m}+\bar{W}_m\cdot\overline{\rho'\cdot W'_n}+\overline{\rho'\cdot W'_m\cdot W'_n})$$
$$-k_n\cdot(\bar{\rho}\cdot\overline{W'^2_n}+2\bar{W}_n\cdot\overline{\rho'\cdot W'_n}+\overline{\rho'\cdot W'^2_n}-\bar{\rho}\cdot\overline{W'^2_m}-2\bar{W}_m\cdot\overline{\rho'\cdot W'_m}-\overline{\rho'\cdot W'^2_m})] \quad (26)$$

Momentum Equation-Normal Direction (-n)

$$\Delta_n=-\frac{1}{b}\cdot\frac{\partial[B\cdot(\bar{\rho}\cdot\overline{W'^2_n}+2\bar{W}_n\cdot\overline{\rho'\cdot W'_n}+\overline{\rho'\cdot W'^2_n})]}{\partial n}$$
$$-\frac{1}{b}\cdot\frac{\partial[B\cdot(\bar{\rho}\cdot\overline{W'_m\cdot W'_n}+\bar{W}_m\cdot\overline{\rho'\cdot W'_n}+\bar{W}_n\cdot\overline{\rho'\cdot W'_m}+\overline{\rho'\cdot W'_m\cdot W'_n})]}{\partial m}$$
$$+\cos\phi(\bar{\rho}\cdot\overline{W'^2_u}+2\bar{W}_u\cdot\overline{\rho'\cdot W'_u}+\overline{\rho'\cdot W'^2_u}+2\omega\cdot R\cdot\overline{\rho'\cdot W'_u})$$
$$-R\cdot[2k_n\cdot(\bar{\rho}\cdot\overline{W'_n\cdot W'_m}+\bar{W}_n\cdot\overline{\rho'\cdot W'_m}+\bar{W}_m\cdot\overline{\rho'\cdot W'_n}+\overline{\rho'\cdot W'_m\cdot W'_n})$$
$$-k_m\cdot(\bar{\rho}\cdot\overline{W'^2_m}+2\bar{W}_m\cdot\overline{\rho'\cdot W'_m}+\overline{\rho'\cdot W'^2_m}-\bar{\rho}\cdot\overline{W'^2_n}-2\bar{W}_n\cdot\overline{\rho'\cdot W'_n}-\overline{\rho'\cdot W'^2_n})] \quad (27)$$

All the above mentioned fluctuation terms (Δ_o, Δ_u, Δ_m, Δ_n) are usually neglected during the calculations presented up to now. A first attempt to simulate these terms was presented by L.H. Smith [15]. The experimental values of the apparent stresses measured at the exit of a transonic rotor were used also by Sehra and Kerrebrock [16] in order to be included in a non-axisymmetric version of their streamline-curvature code. On the other hand Kirschner and Stoff [17] used analytical laws in their effort to include the blade-to-blade flow variations in a semi-inverse design method for supersonic compressor cascades.

4. Apparent Stresses in Bladed Regions

One of the most common assumptions adopted during the investigation of the impact of the apparent stresses is the neglect of the peripheral variation of the flow density, i.e.:

$$\rho' \approx 0 \quad (28)$$

This approximation has its origin on the similar hypothesis of Morkovin as far as the turbulence density fluctuation is concerned, and will be used here for subsonic shear flows due to the lack of detailed experimental data for this flow parameter. In this way the necessary fluctuation terms are significantly simplified. Consequently, the fluctuation terms are given according to equations (24) to (27) as:

$$\Delta_o=0 \quad (29)$$

$$\Delta_u=-\frac{1}{b}\cdot\frac{\partial(B\cdot\bar{\rho}\cdot\overline{W'_m\cdot W'_u})}{\partial m}-\frac{1}{b}\cdot\frac{\partial(B\cdot\bar{\rho}\cdot\overline{W'_n\cdot W'_u})}{\partial n}$$
$$-\cos\phi(\bar{\rho}\cdot\overline{W'_u\cdot W'_n})-R\cdot[k_n\cdot\bar{\rho}\cdot\overline{W'_u\cdot W'_m}+k_m\cdot\bar{\rho}\cdot\overline{W'_u\cdot W'_n}] \quad (30)$$

$$\Delta_m=-\frac{1}{b}\cdot\frac{\partial(B\cdot\bar{\rho}\cdot\overline{W'^2_m})}{\partial m}-\frac{1}{b}\cdot\frac{\partial(B\cdot\bar{\rho}\cdot\overline{W'_m\cdot W'_n})}{\partial n}$$
$$-R\cdot[2k_m\cdot(\bar{\rho}\cdot\overline{W'_n\cdot W'_m})+k_n\cdot(\bar{\rho}\cdot\overline{W'^2_m}-\bar{\rho}\cdot\overline{W'^2_n})] \quad (31)$$

$$\Delta_n=-\frac{1}{b}\cdot\frac{\partial(B\cdot\bar{\rho}\cdot\overline{W'^2_n})}{\partial n}-\frac{1}{b}\cdot\frac{\partial(B\cdot\bar{\rho}\cdot\overline{W'_m\cdot W'_n})}{\partial m}$$
$$+\cos\phi(\bar{\rho}\cdot\overline{W'^2_u})-R\cdot[2k_n\cdot(\bar{\rho}\cdot\overline{W'_n\cdot W'_m}+k_m\cdot(\bar{\rho}\cdot\overline{W'^2_n}-\bar{\rho}\cdot\overline{W'^2_m})] \quad (32)$$

Using the simplified form of these equations we save more than 50% of the computational effort, without any visible change in our results.

As we can easily see from the above equations the following terms ($W_m'^2$, $W_u'^2$, $W_n'^2$, $W_m'.W_u'$, $W_m'.W_n'$, $W_u'.W_n'$) have to be estimated in order to predict the various "Δ_i" terms. For axial configurations and bladed regions the available experimental results were investigated concerning either compressor rotor bladings [18], [19] (e.g. Lakshminarayana et al.,1986, Janssen et al.,1991) or compressor cascades [20], [21] (e.g. Flot,1975, Kaldellis et al.,1990b). Taking into account that inside bladed regions measurements are not available very close to the blade surfaces, we present in figures [4] and [5] the evolution of the peripheral distribution of the $W_m'^2$ component at the inlet, near the mid-chord and near the exit of a highly loaded compressor cascade at two different distances from the wall. As we can easily

see from these figures important meridional velocity fluctuation values are encountered near the blade suction side even at the outer part of the endwall shear layer, due to the blade shear layer. On the other hand the meridional velocity fluctuation is negligible at the mid-passage area and the blade pressure side, excluding the endwall values. Finally, for simulation purposes, all the meridional velocity fluctuation profiles can be described by a second-order polynomial, with minimum at blade mid-passage. Almost the same remarks are also valid for the experimental measurements concerning the peripheral velocity fluctuation profiles $W_u'^2$ and the meridional-peripheral cross product $W_m'.W_u'$. Comparing the meridional and the peripheral fluctuation terms, we can easily observe that the peripheral fluctuation terms present a more symmetrical distribution between the suction and the pressure side of the blades than the meridional fluctuation terms.

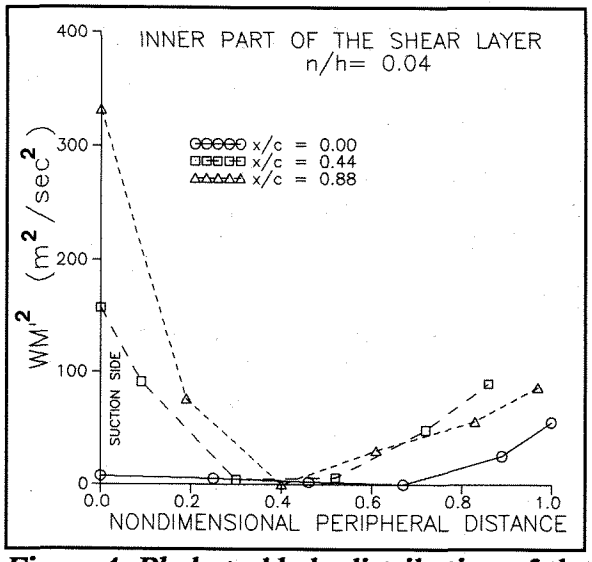

Figure 4: Blade-to-blade distribution of the meridional apparent stresses.

Almost the same results are valid for the experimental data of Lakshminarayana et al. [18] and Janssen et al. [19], concerning the blade-to-blade distribution of the velocity fluctuation components inside a low-speed compressor rotor. Besides, in both cases the meridional velocity fluctuations are bigger than the corresponding peripheral velocity ones. Based also on the above mentioned results we may conclude that the blade-to-blade variation of the principal apparent stresses presents a rather similar behaviour either for stationary or for rotating bladings, excluding cases with shock - shear flow interaction.

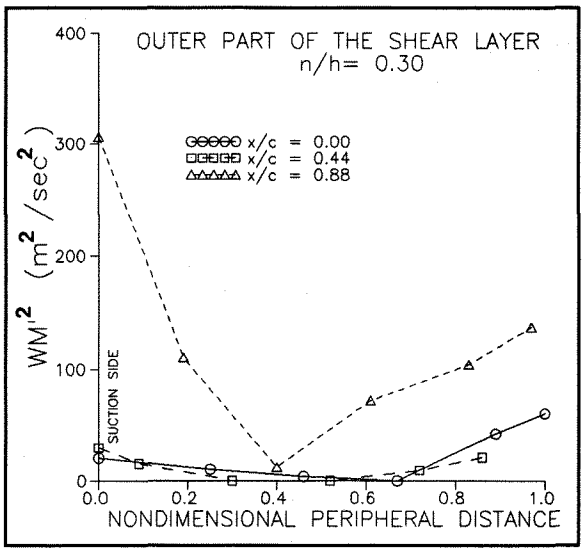

Figure 5: Blade-to-blade distribution of the meridional apparent stresses.

For the calculation of the blade-to-blade variations inside the bladed regions we apply the blade-to-blade shear flow code presented by Katramatos and Kaldellis [2], properly modified in order to include quasi-3-D effects (i.e. "W_n" is constant but not zero at every quasi-3-D axisymmetric surface). The exact values of W_n along with the corresponding values of W_u are predicted using the meridional vorticity field along with the continuity equation for every "S_3" cross-passage section [6] of the computational domain. More precisely:

$$\frac{\partial(R\cdot W_u)}{\partial n}-\frac{\partial W_n}{\partial \theta}=R\cdot\xi_m \qquad (33)$$

and

$$\frac{1}{R}\cdot\frac{\partial W_u}{\partial \theta}+\frac{\partial W_n}{\partial n}=-\frac{1}{\bar{\rho}}\cdot\frac{\partial \bar{\rho}\cdot W_m}{\partial m}-W_n\cdot\left(\frac{\cos\phi}{R}+\frac{\partial \ln\bar{\rho}}{\partial n}+k_m\right)$$
$$-W_m\cdot\left(\frac{\sin\phi}{R}+k_m\right) \qquad (34)$$

The circumferentially mean density and meridional vorticity components are taken from the secondary flow calculation code [1], while the corresponding meridional vorticity is linearly distributed in the peripheral direction. Numerical tests carried out using uniform or cubic distribution of the meridional vorticity in the peripheral direction show only limited influence on the corresponding velocity field, see also [20].

The use of the complete numerical analysis (blade-to-blade fluctuations included) increase by a factor of 3.5 the necessary computational time in comparison with the time needed by the secondary flow method [7] for a highly loaded

compressor cascade, Flot case B'. However, the necessary CPU time is less than two hours on a 25MHz -386 machine.

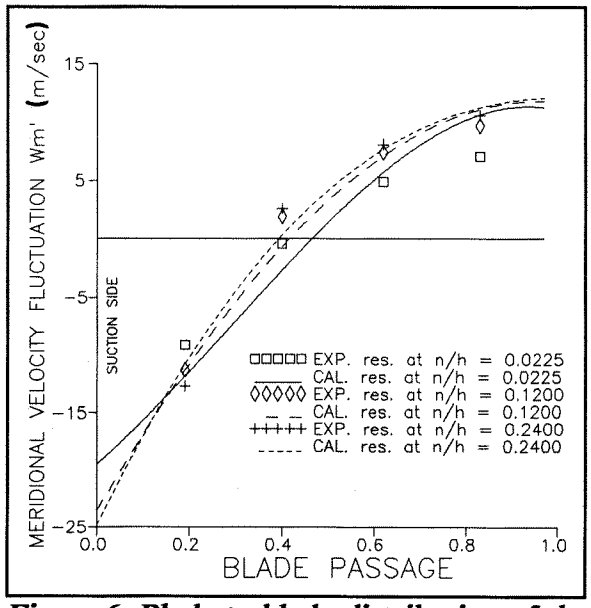

Figure 6: Blade-to-blade distribution of the meridional velocity fluctuations.

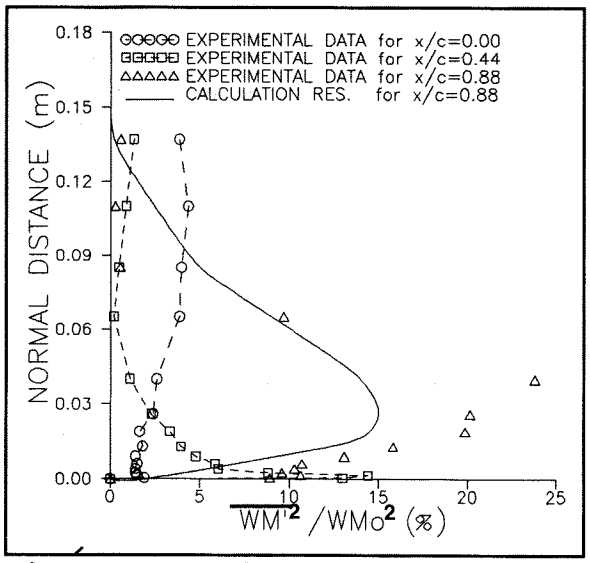

Figure 7: Spanwise distribution of the apparent stresses, throughout a highly loaded compressor cascade.

For comparison purposes in figure [6] the predicted meridional velocity fluctuation profiles near the exit of the cascade are compared with the available experimental data, at various distances from the endwall. As we can easily conclude from this figure the calculation results are reasonably well compared with the experimental measurements, especially after the 5% of the passage height. Mention also that the corresponding normal velocity component is found to be almost one order of magnitude less than the meridional one at the main part of the channel, while the peripheral velocity fluctuation profiles present quite similar behaviour with the meridional ones.

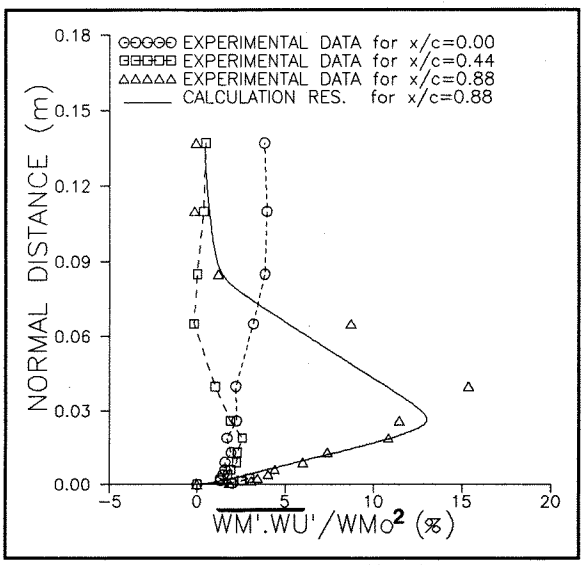

Figure 8: Spanwise distribution of the apparent stresses, throughout a highly loaded compressor cascade.

Finally, since our final target is to evaluate the passage averaged fluctuation terms we present in figures [7] and [8] the experimental and the calculated spanwise distributions of the $\overline{W_m'^2}$ and $\overline{W_m'.W_u'}$ fluctuation terms for the inlet, the mid-chord and near the exit of the cascade. Since the magnitude of the circumferential mean fluctuation terms is comparable with the experimental noise (2%) for the first half of the blade, the calculation results only at the last station are presented. As we can easily conclude, the experimental trends are rather well reproduced by the proposed calculation procedure, although the position and the exact value of the maximum of the profiles of the apparent stresses are slightly underpredicted.

5. Apparent Stresses in Unbladed Regions

The main body of the experimental work presented up to now for the blade-to-blade variation of the flow velocity components was carried out for unbladed regions downstream of the trailing edge of the preceding blading. Among the most interesting results presented are the measurements given by Sehra and Kerrebrock [16] concerning the apparent stresses spanwise distribution 0.1 and 1.0 chord downstream of a transonic rotor. Detailed experimental investigations was carried out also by Jadayel and

Railly (1989) for axial compressor rotors [21] and by Leylek and Wisler, 1991 with emphasis on the "radial mixing" in axial flow compressors [22].

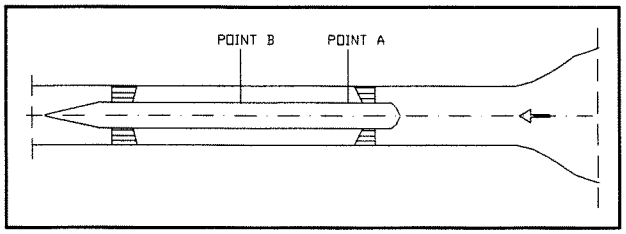

Figure 9: Schematic representation of the experimental high velocity separator.

In the present analysis besides the available experimental data for the above mentioned transonic rotor [16] we take into account detailed measurements carried out downstream of the "Flot case B'" highly loaded compressor cascade [8], [20] and the corresponding experimental results concerning a high velocity separator, see also Cerdan and Talleu [23], and Ktenidis and Kaldellis, [24], where measurements are taken 1/3 and 5 chords downstream of the biparabolic distributing blades, figure [9]. The inlet velocity is constant and equal to 50m/sec, while the distributing blades are followed by circular type straightening blades.

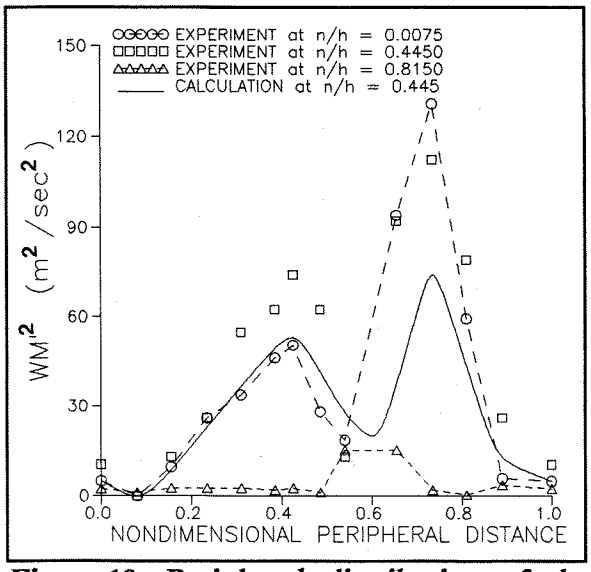

Figure 10: Peripheral distribution of the meridional apparent stresses inside the wake.

For the calculation of the peripheral distribution of the velocity fluctuation components we use the theoretical model proposed for bladed regions, with the additional assumption that the meridional flow angle "β" inside the free spaces keeps the corresponding value at the blading trailing edge. This assumption is utilized here instead of developing a complete 3-D asymmetric wake model, which is now under progress. An additional modification is included in the pitchwise distribution of the meridional vorticity, using exponentially decreasing functions, in order to modify the linear peripheral variation of the meridional vorticity utilized inside bladed regions to a uniformly distributed one, one chord downstream of the blading trailing edge.

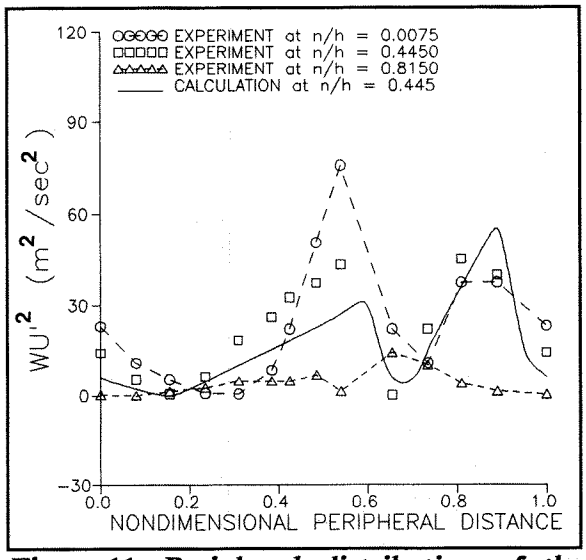

Figure 11: Peripheral distribution of the peripheral apparent stresses inside the wake.

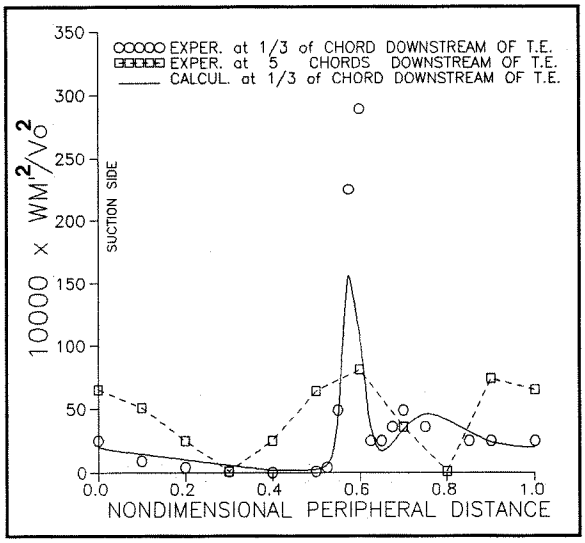

Figure 12: Distribution of the meridional apparent stresses, H.V.S.

The calculation results describe relatively well the experimental distributions of the $W_m'^2$, $W_u'^2$ and $W_{m'}.W_u'$ in the peripheral direction (for one blade passage) at various distances from the wall, see for example figures [10] to [11], for the compressor

cascade test case. According to the results presented in these two figures the flow quantities are almost uniformly distributed at the central part of the flow field, while even inside the endwall shear layer region the apparent stresses are quite small. Another interesting flow aspect is that the maximum values of the $W_m'^2$ component almost coincide with the minimum values of $W_u'^2$ component and vice-versa.

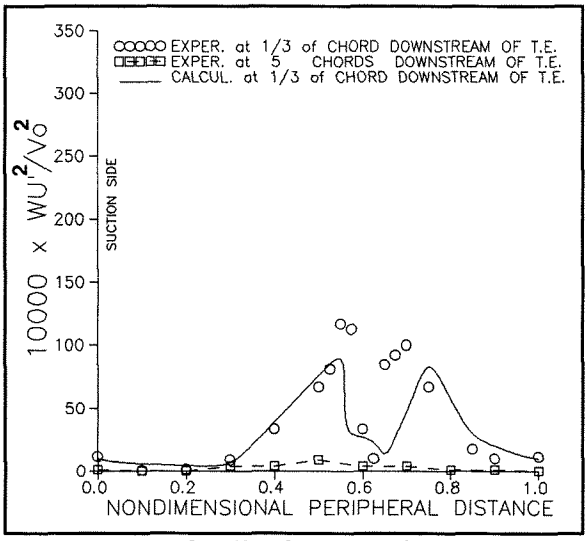

Figure 13: Distribution of the peripheral apparent stresses, H.V.S.

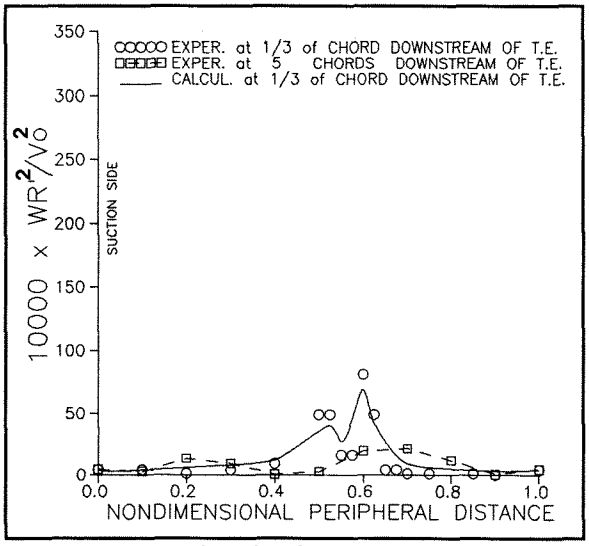

Figure 14: Distribution of the normal apparent stresses, H.V.S.

The same remark is also valid for the maximum and minimum values of the apparent stresses distribution at the mid-span of the high velocity separator one third of axial chord downstream of the blading trailing edge, see figures [12] and [13]. The maximum value of the corresponding radial velocity component, figure [14], is much smaller (1:6) than the meridional one. Five blade chords

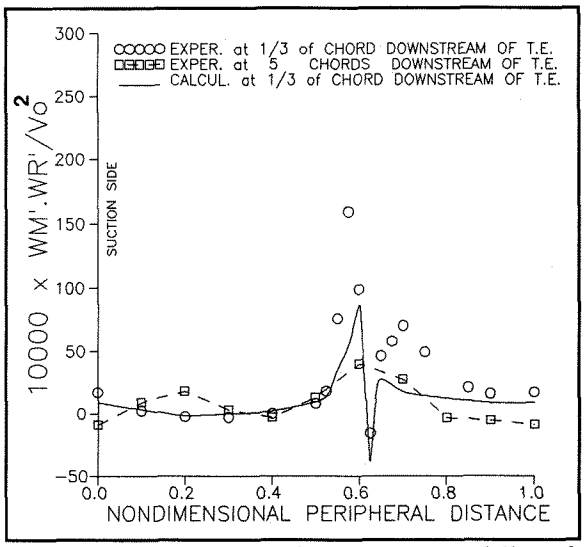

Figure 15: Distribution of meridional-normal apparent stresses, H.V.S.

downstream of the blade trailing edge all the apparent stresses are almost vanished, except the meridional $W_m'^2$, and meridional-radial cross product $W_m'.W_r'$ peripheral distributions, see figures [12] to [15]. Again the calculation results describe the experimental points with enough accuracy for engineering purposes. The existence of two maximum in the peripheral distribution of the normal apparent stresses is in accordance with the presence of remarkable asymmetric wakes.

6. Conclusions

A non-axisymmetric 3-D viscous flow analysis was presented, in order to describe the most important terms produced by the circumferential integration of the flow quantities. Detailed experimental data for stationary bladings were analyzed with emphasis on the flow non-uniformities in the peripheral direction. Besides, the investigated experimental flow pattern was found quite similar with the available measurements from other experiments existing in the literature, for rotating and stationary bladings.

Next, the non-axisymmetric flow terms are gathered in two groups, the deficit force terms and the apparent stress ones. For both categories a consistent theoretical model was presented and accordingly applied, and the calculation results describe quite realistically the experimental data, for bladed and unbladed regions.

Additionally, the relative importance of all these terms was discussed, without however to have the ability to decide with certainness about the importance of the six apparent stress components encountered. Therefore, all these terms will be taken into account during the application of the

complete method, non-axisymmetric terms included, in future work. On the other hand, the meridional and the peripheral deficit force components were found to take important values especially for the first half of the blade. Both pressure and stress blade force components are included in our study. Finally, special attention was paid since the relations existing between the three deficit force components set at the same time implicit constraints between the loss distribution in the three directions.

References

1. Kaldellis J., Douvikas D., Falchetti F., Papailiou K., 1990, "A Secondary Flow Calculation Method for One Stage Axial Transonic Flow Compressors, Including Shock-Secondary Flow Interaction", ASME Jr. of Turbomachinery, Vol. 112, pp.652.

2. Katramatos D., Kaldellis J., 1991, "3-D Loss Prediction Based on Secondary Flow and Blade Shear Layer Interaction", ASME Paper 91-GT-59, Orlando, USA.

3. Kaldellis J.,1993, "Parametrical Investigation of the Interaction Between Turbulent Wall Shear Layers and Normal Shock Waves, Including Separation", ASME Journal of Fluids Engineering, Vol.115.

4. Kaldellis J., Georgantopoulos G., 1994, "Investigation of Shear Layer Transition using Various Turbulence Models", AGARD 74th Fluid Dynamics Panel, Chania, Greece.

5. Kaldellis J.,1994, "Energy Exchange and Loss Prediction in Axial Turbines and Compressors", presented at the FLOWERS'94 Conference, Firenze, Italy.

6. Vavra M.H., 1974,"Aero-Thermodynamics & Flow in Turbomachines", Robert E., Krieger Publishing Company, New York.

7. Kaldellis J., Douvikas D., Papailiou K.,1988, "A Secondary Flow Calculation Method Based on the Meridional Vorticity Transport Equation", ASME Paper 88-GT-260, Amsterdam.

8. Flot R., 1975, "Contribution a l' Etude des Ecoulements Secondaires dans les Compresseurs Axiaux", These de Docteur Ingenieur, Lyon I.

9. Storer J.A., Cumpsty N.A., 1990, "Tip Leakage Flow in Axial Compressors", ASME Paper 90-GT-127.

10. Hawthorne W.R., 1964, "Aerodynamics of Turbines and Compressors", Princeton University Press.

11. Kaldellis J., Ktenidis P., 1990, "High Turning Limit and Jet Like Profiles in Secondary Flow Field of Axial Turbines", ASME Paper 90-GT-327, Brussels.

12. Brochet J., Falchetti F., 1987, "Secondary Flow Computation in Multistage Axial Flow Compressors", 8th ISABE Conf, USA.

13. Comte A., Ohayon G., Papailiou K., 1981, "A Method for the Calculation of the Wall Layers Inside the Passage of a Compressor Cascade with and Without Tip Clearance", ASME Paper 81-GT-168, USA.

14. Mellor G.L., Wood G.M., 1971, "An Axial Compressor End-Wall Boundary Layer Theory", ASME Jr. of Basic Eng., Vol.93.

15. Smith Jr. L.H., 1966, "The Radial-Equilibrium Equation of Turbomachinery", ASME Jr. of Eng. for Power, Series A, Vol.88, pp.1-12.

16. Sehra A.K., Kerrebrock J.L., 1979, "The Effect of Blade-to-Blade Flow Variations on the Mean Flow-Field of a Transonic Compressor", AIAA Paper 79-1515, Virginia, USA.

17. Kirschner A., Stoff H., 1990, "Semi-Inverse Design of Compressor Cascades, Including Supersonic Inflow", ASME Paper 90-GT-237, Brussels, Belgium.

18. Lakshminarayana B., Sitaram N., Zhang J., 1986, "End-Wall and Profile Losses in a Low-Speed Axial Flow Compressor Rotor", ASME Jr. of Eng. for Gas Turbines and Power, Vol.108, No1, pp.22-31.

19. Janssen M., Dohmen H.J., Grahl K.G., 1991, "Computation of 3-D Flow Phenomena in Axial Flow Compressor Blade Rows", ASME Paper 91-GT-78, Orlando, USA.

20. Kaldellis J., Papadopoulos P., Kodossakis D., 1990, "Non-Axisymmetric Terms in Secondary Flow Analysis of Bladed Regions. Theory and Experiments.", Internal Note, University of Piraeus, IT90-TURB13, Greece.

21. Jadayel O.C., Railly J.W., 1989, "A Theoretical and Experimental Investigation of the Reynolds and Apparent Stresses in Axial Compressors", presented in 9th ISABE Conference, Athens, Greece.

22. Leylek J.H., Wisler D.C., 1991, "Mixing in Axial-Flow Compressors: Conclusions Drawn from Three-Dimensional Navier-Stokes Analyses and Experiments", ASME Jr. of Turbomachinery, Vol.113.

23. Cerdan J.P., Talleu P., 1981, "The High Velocity Separators: A New Progress in Steam-Water Separation Technology", Paper presented at the International Symposium on "Applications of Fluid Mechanics and Heat Transfer to Energy and Environmental Problems", Vol.III, Greece.

24. Ktenidis P., Kaldellis J., 1991, ""Non-Axisymmetric Terms in Secondary Flow Analysis of Internal Unbladed Regions. Theory and Experiments.", Internal Note, Un.of Piraeus, IT91-TURB16, Greece.

Appendix One

The governing equations used in the present work after the use of the CAM are written in an orthogonal curvilinear axisymmetric coordinate system as :

Mass Conservation Equation

$$\frac{1}{b}\cdot\left[\frac{\partial}{\partial m}(b\cdot R\cdot\bar{\rho}\cdot\bar{W}_m)+\frac{\partial}{\partial n}(b\cdot R\cdot\bar{\rho}\cdot\bar{W}_n)\right]+R\cdot(k_n\cdot\bar{\rho}\cdot\bar{W}_m+k_m\cdot\bar{\rho}\cdot\bar{W}_n)+\Delta_o=0 \quad (1.1)$$

Momentum Equation-Peripheral Direction

$$\begin{aligned}&\frac{1}{b}\cdot\frac{\partial(B\cdot\bar{\rho}\cdot\bar{W}_m\cdot\bar{W}_u)}{\partial m}+\frac{1}{b}\cdot\frac{\partial(B\cdot\bar{\rho}\cdot\bar{W}_n\cdot\bar{W}_u)}{\partial n}+\cos\phi(\bar{\rho}\cdot\bar{W}_u\cdot\bar{W}_n\\&+2\omega\cdot R\cdot\bar{\rho}\cdot\bar{W}_n)+\sin\phi(\bar{\rho}\cdot\bar{W}_u\cdot\bar{W}_m+2\omega\cdot R\cdot\bar{\rho}\cdot\bar{W}_m)=F_u+\Delta_u\\&-R\cdot(k_n\cdot\bar{\rho}\cdot\bar{W}_u\cdot\bar{W}_m++k_m\cdot\bar{\rho}\cdot\bar{W}_u\cdot\bar{W}_n)\frac{1}{b}\cdot\frac{\partial(B\cdot\bar{\tau}_{mu})}{\partial m}+\frac{1}{b}\cdot\frac{\partial(B\cdot\bar{\tau}_{nu})}{\partial n}\\&+R\cdot(k_n\cdot\bar{\tau}_{nu}+k_m\cdot\bar{\tau}_{mu})+\bar{\tau}_{uu}\cdot\cos\phi+\bar{\tau}_{nu}\cdot\sin\phi\end{aligned} \quad (1.2)$$

Momentum Equation-Meridional Direction

$$\begin{aligned}&\frac{1}{b}\cdot\frac{\partial(B\cdot\bar{\rho}\cdot\bar{W}^2_m)}{\partial m}+\frac{1}{b}\cdot\frac{\partial(B\cdot\bar{\rho}\cdot\bar{W}_m\cdot\bar{W}_n)}{\partial n}-\sin\phi(\bar{\rho}\cdot\bar{W}^2_u+\bar{\rho}\cdot\omega^2\cdot R^2\\&+2\omega\cdot R\cdot\bar{\rho}\cdot\bar{W}_u)=-\frac{R}{b}\cdot\frac{\partial(b\cdot\bar{p})}{\partial m}+F_m+\Delta_m-R\cdot[2k_m\cdot\bar{\rho}\cdot\bar{W}_n\cdot\bar{W}_m\\&-k_n\cdot(\bar{\rho}\cdot\bar{W}^2_n-\bar{\rho}\cdot\bar{W}^2_m)]+\frac{1}{b}\cdot\frac{\partial(B\cdot\bar{\tau}_{mm})}{\partial m}+\frac{1}{b}\cdot\frac{\partial(B\cdot\bar{\tau}_{nm})}{\partial n}\\&-\bar{\tau}_{uu}\cdot\sin\phi+R\cdot[k_n\cdot(\bar{\tau}_{mn}-\bar{\tau}_{nn})+k_m\cdot(\bar{\tau}_{mn}+\bar{\tau}_{nm})]\end{aligned} \quad (1.3)$$

Momentum Equation-Normal Direction (-n)

$$\begin{aligned}&\frac{1}{b}\cdot\frac{\partial(B\cdot\bar{\rho}\cdot\bar{W}^2_n)}{\partial n}+\frac{1}{b}\cdot\frac{\partial(B\cdot\bar{\rho}\cdot\bar{W}_m\cdot\bar{W}_n)}{\partial m}-\cos\phi(\bar{\rho}\cdot\bar{W}^2_u+\bar{\rho}\cdot\omega^2\cdot R^2\\&+2\omega\cdot R\cdot\bar{\rho}\cdot\bar{W}_u)=-\frac{R}{b}\cdot\frac{\partial(b\cdot\bar{p})}{\partial n}+F_n+\Delta_n-R\cdot[2k_n\cdot\bar{\rho}\cdot\bar{W}_n\cdot\bar{W}_m\\&-k_m\cdot(\bar{\rho}\cdot\bar{W}^2_m-\bar{\rho}\cdot\bar{W}^2_n)]+\frac{1}{b}\cdot\frac{\partial(B\cdot\bar{\tau}_{mn})}{\partial m}+\frac{1}{b}\cdot\frac{\partial(B\cdot\bar{\tau}_{nn})}{\partial n}\\&-\bar{\tau}_{uu}\cdot\cos\phi+R\cdot[k_m\cdot(\bar{\tau}_{nn}-\bar{\tau}_{mm})+k_n\cdot(\bar{\tau}_{mn}+\bar{\tau}_{nm})]\end{aligned} \quad (1.4)$$

The energy conservation and the transport of vorticity equation in the meridional direction are not presented here, since they used in the form already given [1] by Kaldellis et al.,1990.